rotation (in this case carried out by the Kaiser varimax procedure) the three eigenvectors all corresponded to distortions with C_{2v} cokernel symmetry. The relation between bond and angle deformations is easily seen from the appropriate components of the factors. Thus as r_1 and r_4 increase by 0·55 standard deviations (bond), r_2 and r_3 decrease by the same amount, α_{14} decreases by 0·89 standard deviations (angle) and α_{23} increases by the same amount. Multiplying these quantities by the observed standard deviations (Table 2*a*) we find that for a change of 1° in α_{14} there is a corresponding decrease in bond length r_1 of 0·0063 Å, very similar to the results of MBD*b* from correlation of symmetry coordinates.

References

BAUR, W. H. (1974). *Acta Cryst.* B**30**, 1195–1215.

BÜRGI, H.-B. (1975). *Angew. Chem. Ind. Ed. Engl.* **14**, 460–473.

BÜRGI, H.-B., DUNITZ, J. D. & SHEFTER, E. (1973). *J. Am. Chem. Soc.* **95**, 5066–5067.

DUNITZ, J. D. (1975). *Proc. R. Soc. London Ser. B*, **272**, 99–108.

MCDOWELL, R. S. (1965). *J. Mol. Spectrosc.* **17**, 365–367.

MURRAY-RUST, P. & BLAND, R. (1978). *Acta Cryst.* B**34**, 2527–2533.

MURRAY-RUST, P., BÜRGI, H.-B. & DUNITZ, J. D. (1975). *J. Am. Chem. Soc.* **97**, 921–922.

MURRAY-RUST, P., BÜRGI, H.-B. & DUNITZ, J. D. (1978*a*). *Acta Cryst.* B**34**, 1787–1793.

MURRAY-RUST, P., BÜRGI, H.-B. & DUNITZ, J. D. (1978*b*). *Acta Cryst.* B**34**, 1793–1803.

MURRAY-RUST, P., BÜRGI, H.-B. & DUNITZ, J. D. (1979). *Acta Cryst.* A**35**, 703–713.

MURRAY-RUST, P. & MOTHERWELL, W. D. S. (1978*a*). *Acta Cryst.* B**34**, 2518–2526.

MURRAY-RUST, P. & MOTHERWELL, W. D. S. (1978*b*). *Acta Cryst.* B**34**, 2534–2546.

WILSON, E. B., DECIUS, J. C. & CROSS, P. C. (1955). *Molecular Vibrations*. New York: McGraw-Hill.

Acta Cryst. (1982). B**38**, 2771–2775

Neutron Diffraction Study of the Crystallographic and Magnetic Structures of Potassium Tribromoferrate(II)

BY E. GUREWITZ

Nuclear Research Centre–Negev, POB 9001, *Beer Sheva* 84190, *Israel*

AND H. SHAKED

Nuclear Research Centre–Negev, and Ben-Gurion University of the Negev, POB 653, *Beer Sheva* 84120, *Israel*

(*Received* 7 *October* 1981; *accepted* 9 *February* 1982)

Abstract

A neutron diffraction study of a powder sample of $KFeBr_3$ was carried out at various temperatures. (Weighted R factors are 0·076, 0·075 for 26, 31 intensities measured at room temperature and liquid-helium temperature, respectively.) This compound was found to be isostructural with $KFeCl_3$ and belongs to the orthorhombic space group *Pnma* with four molecules per unit cell. It is paramagnetic at room temperature and undergoes a transition to a magnetically ordered state at $T_N \sim 9{\cdot}5$ K. The magnetic structure as determined from diffraction patterns at 4·2 K consists of antiferromagnetically coupled ferromagnetic chains parallel to **b**. The antiferromagnetic axis is along **b** and the magnetic moment per Fe^{2+} ion is $3{\cdot}7 \pm 0{\cdot}2$ BM (1 BM $\equiv 9{\cdot}27 \times 10^{-24}$ J T^{-1}). The temperature dependence of the magnetic reflections shows some residual coherent reflections above T_N. This is interpreted in terms of strong one-dimensional intrachain correlations.

I. Introduction

Most of the ABX_3 compounds, where A is an alkaline metal, B a transition metal and X a halogen or O, have crystallographic structures which are derived from either the ideal cubic perovskite or the hexagonal perovskite structures. However, some ABX_3 compounds have different structures. For example, the structure of $KCdCl_3$ (Wyckoff, 1964) cannot be obtained from the cubic or the hexagonal perovskite-like structures by a series of continuous distortions.

The compounds $KFeCl_3$ and $KFeBr_3$ are isostructural with $KCdCl_3$ (Gurewitz, Makovsky &

0567-7408/82/112771-05$01.00

Shaked, 1974; Amit, Horowitz & Makovsky, 1974). This structure consists of isolated zigzagging chains (ZC) of $CdCl_3$ octahedra. As a consequence of their crystallographic structure, these compounds exhibit one-dimensional magnetic correlations at low temperature. These one-dimensional correlations are different from those in other known one-dimensional magnetically correlated compounds in having four nearest neighbours rather than two. These correlations show up in a neutron scattering experiment upon cooling the sample at $T_N < T < 2T_N$. At T_N long-range three-dimensional magnetic ordering sets in, as exhibited by a sharp increase in the magnetization upon cooling. The present work is a study of the crystallographic and magnetic structures of $KFeBr_3$.

II. Preparation and crystallographic structure

The compound $KFeBr_3$ was prepared as follows. Stoichiometric amounts of the appropriate potassium and ferrous bromides were mixed and loaded into evacuated quartz ampoules. The loaded ampoules were sealed and annealed at 873 K for several hours. An analysis of the room-temperature (RT) X-ray powder diagram of a sample from this preparation (Amit, Horowitz & Makovsky, 1974) showed that it is isostructural with $KCdCl_3$ (Wyckoff, 1964). The unit-cell dimensions as calculated from the X-ray data are $a = 9{\cdot}220\ (6)$, $b = 4{\cdot}026\ (8)$, $c = 14{\cdot}899\ (9)$ Å, which are slightly greater than those for $KFeCl_3$.

The neutron diffraction powder pattern of a sample of $KFeBr_3$ at room temperature is shown in Fig. 1(*a*). Some additional weak reflections due to the presence of a small amount of $FeBr_2$ are observed. This pattern is very similar to that obtained for $KFeCl_3$ (Gurewitz, Makovsky & Shaked, 1974) and we therefore assume that the two compounds are isostructural. Hence, the structure of $KFeBr_3$ belongs to the orthorhombic space group *Pnma* (D_{2h}^{16}) with four molecules per unit cell. All the ions occupy the special positions 4(*c*) with point symmetry *m*. The position parameters *x* and *z*, for all the ions, were calculated by fitting the calculated intensities to the integrated observed ones using a least-squares computer program. The background at each reflection was determined by fitting a high-order polynomial function to the background throughout the spectrum. Separations of peaks into groups of reflections were made when the interval between the groups contained only reflections of expected negligible intensities. In these cases the smooth line through the data points at either the leading or tailing edge, modified by the Lorentz factor, was used to construct the intensity contour for the entire group. The best fit of the calculated intensities to the integrated observed ones is given in Table 1. The parameters yielding this best fit are given in Table 2. These parameters are similar to

Table 1. *Comparison of calculated and observed integrated intensities of neutrons* ($\lambda \sim 1{\cdot}02$ Å) *reflected from a powder sample of* $KFeBr_3$ *at RT*

hkl	Integrated intensities Observed	Calculated
101 002	126 ± 6	126
102*	74 ± 10	75
200	15 ± 3	12
201 103	3 ± 3	3
202	3 ± 2	3
011	3 ± 3	4
004	6 ± 3	10
111	17 ± 2	22
104	2 ± 2	2
203	18 ± 3	20
112*	20 ± 3	20
013*	2 ± 2	2
210 301 211 113	222 ± 10	222
204*	88 ± 6	88
302 105 212	224 ± 10	207
114 303 213	26 ± 3	23
205 006	16 ± 3	11
311 106 015	77 ± 5	76
304 214 312 115 400 401	Obscured	46
402 313 206	22 ± 3	20
305 215	14 ± 4	10
403 107 116*	48 ± 5	53
020 410	Obscured	89
411	2 ± 2	1
404 121 207 022 306 412 216	81 ± 4	82
122 315 017 008 413 117 220 501 108 221 123*	178 ± 7	185
502 222 024 414 307 217 316 124 503 208 223*	43 ± 14	55
406 321 511 118 415 504 224 322 125 512 109	116 ± 8	109

* These reflections include small contributions from $FeBr_2$ impurity.

Table 2. *Parameters for* $KFeBr_3$ [*Pnma* (D_{2h}^{16})] *refined with the RT and LHT data*

Ion	Parameters[a]	RT	LHT
Fe^{2+}	*x*	0·175 ± 0·002	0·169 ± 0·003
	z	0·052 ± 0·006	0·058 ± 0·003
K^+	*x*	0·468 ± 0·017	0·483 ± 0·017
	z	0·822 ± 0·006	0·831 ± 0·007
Br_I	*x*	0·275 ± 0·006	0·287 ± 0·005
	z	0·207 ± 0·003	0·217 ± 0·005
Br_{II}	*x*	0·166 ± 0·006	0·173 ± 0·006
	z	0·495 ± 0·003	0·496 ± 0·003
Br_{III}	*x*	0·015 ± 0·008	0·020 ± 0·009
	z	0·902 ± 0·003	0·904 ± 0·004
Number of Bohr magnetons[b]		—	3·720 ± 0·150
Debye–Waller factor (Å²)		2·1 ± 0·5	1·0 ± 0·5
Weighted *R* factor[c]		0·076	0·075

(*a*) All ions are at the 4(*c*) positions.

(*b*) The number of Bohr magnetons at RT was set equal to 0. The form factors for Fe^{2+} magnetic reflections were taken from Watson & Freeman (1961).

(*c*) $R = \{\sum |(I_{obs} - I_{calc})/\sigma|^2 / \sum |I_{obs}/\sigma|^2\}^{1/2}$; the σ's are the estimated errors in I_{obs} and are given in Tables 1 and 5.

Table 3. *Interatomic distances* (Å) (*e.s.d.'s are* ~0·003 Å) *within a distorted* $KFeBr_3$ *octahedron and comparison with the corresponding distance within the* $FeBr_2$ *ideal octahedron*

Position	Ion	$KFeBr_3$ Br_I	Br_{II}	Br_{III}	Br_{III}	$FeBr_2$ Br
$x,\frac{1}{4},z$	Fe^{2+}	2·490	2·622	2·677	2·744	2·164
$x,\frac{1}{4},z$	Br_I^-		3·568	5·141	3·715	
$\frac{1}{2}-x,\frac{3}{4},\frac{1}{2}+z$	Br_{II}^-			3·820	3·564	3·774
$x,\frac{1}{4},z$	Br_{III}^-				3·552	
$x,\frac{3}{4},z$	Br_{III}^-					

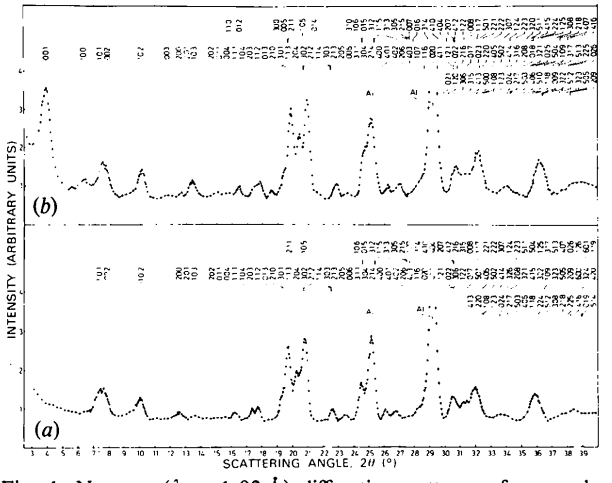

Fig. 1. Neutron (λ ~ 1·02 Å) diffraction patterns of a powder sample of $KFeBr_3$ at (*a*) 300 K and (*b*) 4·2 K. Indexing is according to the orthorhombic unit cell with a = 9·220 (6), b = 4·026 (8) and c = 14·899 (9) Å.

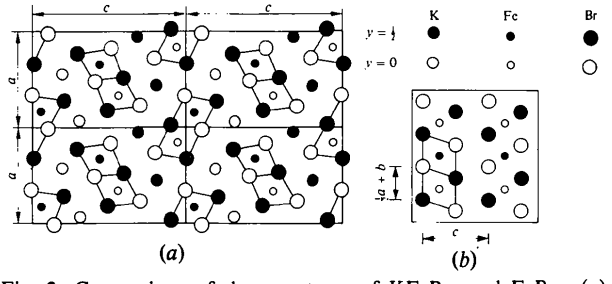

Fig. 2. Comparison of the structures of $KFeBr_3$ and $FeBr_2$. (*a*) (010) projection of the $KFeBr_3$ structure. (*b*) (010) projection of the $FeBr_2$ structure. The lines through the Br circles are the projections of a zigzagging chain.

those obtained for $KFeCl_3$ (Gurewitz, Makovsky & Shaked, 1974) and $KMnCl_3$ (Gurewitz, Horowitz & Shaked, 1979). Each Fe^{2+} ion in this structure is surrounded by a distorted octahedron of Cl^- ions. The octahedra are packed in isolated ZC along **b**, with two ZC in a unit cell (Fig. 2*a*). Each octahedron shares an edge with each of its four neighbouring octahedra. The relation between the packing of the $[FeBr_3]^-$ octahedra in $KFeBr_3$ ZC's and the packing of the $FeBr_2$ octahedra in the hexagonal $FeBr_2$ structure is shown in Fig. 2(*b*). The ZC's are extended, in $FeBr_2$, to form a plane (perpendicular to **c**, see Fig. 2*b*) of a hexagonal network of octahedra, where the orthorhombic **b** translation is approximately the hexagonal **b** translation. The interatomic distances within a distorted octahedron of the ZC structure are given in Table 3 and are compared to their analogous distances in the ideal $FeBr_2$ octahedron.

III. Magnetic structure

Neutron diffraction patterns of a powder sample of $KFeBr_3$ at liquid-helium temperature (LHT) are shown in Fig. 1(*b*). This pattern exhibits the same characteristics as that obtained for $KFeCl_3$ at LHT. Comparison between the RT and the LHT patterns reveals an intensity increase in the following reflections: 001, 100, 101, 102, 003, 201, 103, 202, 011, 012, 104, 112, 301, 005, 211, 113, 204, 302, 105, 212, 014. All these reflections are indexed with respect to the original RT unit cell.

We restrict the search to collinear magnetic structures having the highest possible symmetry. These belong to subgroups of order two of the paramagnetic group $Pnma \times 1'$ and are listed in Table 4. According to this table the existence of the magnetic reflections $0kl$ with $k + l$ odd and $hk0$ with h odd leads to a single magnetic configuration which is the C configuration. A single configuration in the orthorhombic group leads to spins collinear with one of the three orthorhombic axes. The $00l$ and $h00$ magnetic reflections require a nonvanishing **b** component in the magnetic moment. Hence, the magnetic structure is C_y. This structure consists of ferromagnetic ZC's with moments parallel

Table 4. *Definitions of the magnetic configurations and classification of the limiting conditions on allowed magnetic reflections and of the magnetic groups, according to the magnetic configuration* [*space group Pbnm, special position* 4(*c*) (*Gurewitz & Shaked,* 1972)]

Magnetic configuration					Limiting conditions		Magnetic groups		
Configuration	E	2_y	m_x	m_z	$0kl$	$hk0$	$\mathbf{M}\parallel\hat{x}$	$\mathbf{M}\parallel\hat{y}$	$\mathbf{M}\parallel\hat{z}$
	m_y	$\bar{1}$	2_z	2_x					
G	+	−	+	−	$k+l=2n$	$h=2n+1$	$nm'a$	$n'ma$	$n'm'a'$
A	+	−	−	+	$k+l=2n+1$	$h=2n$	$n'm'a'$	nma'	$nm'a$
C	+	+	−	−	$k+l=2n+1$	$h=2n+1$	$n'm'a$	nma	$nm'a'$
F	+	+	+	+	$k+l=2n$	$h=2n$	$nm'a'$	$n'ma'$	$n'm'a$

Table 5. *Comparison of calculated and observed integrated intensities of neutrons* ($\lambda \sim 1{\cdot}02$ Å) *reflected from a powder sample of* $KFeBr_3$ *at LHT*

hkl	Integrated intensities Observed	Calculated
001	427 ± 20	409
100	29 ± 8	41
101 002	150 ± 10	157
102*	97 ± 8	92
003	5 ± 4	9
200	12 ± 4	10
201 103	52 ± 5	56
202 011	17 ± 4	24
004 110	14 ± 3	14
111 012	22 ± 3	21
104	2 ± 2	3
203 112*	54 ± 6	50
013*	12 ± 3	17
210 301 005 211 113	251 ± 10	257
204*	123 ± 6	123
302 105 212	261 ± 10	257
014	10 ± 5	9
114 303 213	31 ± 4	31
205 006	11 ± 5	11
310	2 ± 2	0
311 106 304 214 312 115 400	Obscured	141
401	0 ± 2	2
402 313 206	36 ± 4	32
305 007 215 016 403 107 116 314 020 410	Obscured	316
411 021	9 ± 3	10
404	8 ± 3	10
120 121 207 022 306 412 216	110 ± 8	105
122 315 017*	44 ± 8	52
008 413 023 117 500 220 108 405 221 123 501	170 ± 10	169
502 222	18 ± 4	17
024 414 307 217 316 124 503 208 223*	38 ± 7	51
406 018	0 ± 3	4
320 510 321 511 118 025 415 009 504 224 322 125 512 109	149 ± 10	146

* These reflections include small contributions from $FeBr_2$ impurity.

to the ZC axis. The ZC's are antiferromagnetically coupled. The position parameters x and z, for all the ions, and the magnitude of the magnetic moment were calculated by fitting the calculated intensities to the integrated observed ones using a least-squares computer program. The calculated intensities for the best fit at LHT are given in Table 5, and the parameters yielding the best fit are given in Table 2. The refined value of the magnetic moment at LHT is $3{\cdot}7 \pm 0{\cdot}2$ BM per Fe^{2+} ion,

The intensity–temperature curve of the 001 magnetic reflection is shown in Fig. 3. The curve can be divided into three regions corresponding to three different magnetic phases: (*a*) high temperature (23 K $< T <$ RT), (*b*) intermediate temperature (9·5 K $\leq T <$ 23 K), and (*c*) low temperature ($T \leq$ 9·5 K). In the

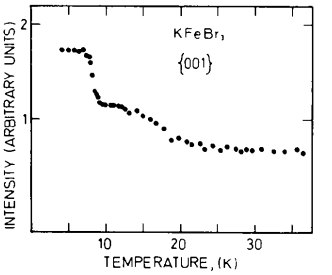

Fig. 3. Temperature dependence of the magnetic 001 reflection of $KFeBr_3$.

high-temperature region the intensity of the magnetic reflection vanishes and the phase is paramagnetic. In the intermediate region the intensity of the magnetic reflection gradually increases as temperature decreases. This indicates that the sample at this phase has appreciable magnetic correlations. The third region starts at the Néel temperature $T_N = 9{\cdot}5$ K where there is an abrupt intensity increase. In this region, there are coherent magnetic contributions to many reflections as observed in the LHT pattern (Fig. 1*b*). Hence, this phase has long-range antiferromagnetic order.

IV. Discussion

The compound $KFeBr_3$ is paramagnetic at temperatures above 23 K. Below $T_N = 9{\cdot}5$ K it orders antiferromagnetically. In the antiferromagnetic state the amounts in each ZC are ferromagnetically coupled while two adjacent ZC's are coupled antiferromagnetically. The structure of a ZC in $FeBr_2$ is of the same form as the structure of a ZC in $KFeBr_3$. In $FeBr_2$ the intrachain Fe—Br—Fe angles (90°) favour a ferromagnetic superexchange. In $KFeBr_3$ the intrachain Fe—Br—Fe angle is 98° which also leads to a ferromagnetic superexchange. The magnetic structure belongs to the magnetic space group *Pnma* (Table 4).

The intrachain distance between two Fe^{2+} neighbours is half the interchain distance which requires a double superexchange coupling. This manifests itself in the intermediate temperature range (9·5 K $\leq T <$ 23 K) by strong ferromagnetic correlations within a ZC while essentially there are no correlations between the ZC's. These correlations are, however, one-dimensional in character and cannot lead to a long-range order. Mössbauer-effect measurements on the isostructural compound $KFeCl_3$ (Gurewitz, Makovsky & Atzmony, 1976) exhibit, in the intermediate temperature range ($T_N \leq T \leq 2T_N$), a typical relaxation character. The relaxation phenomenon was interpreted as follows: the large anisotropy of the crystal constrains the Fe^{2+} moments to be either parallel or antiparallel to the **b** direction. As long as the correlations between the

moments are one-dimensional they are of finite length. Therefore, each chain consists of domains of parallel moments; the direction of the moments at each domain is antiparallel to the direction of the moments in its adjacent domains. The domain boundary point moves along the chain giving rise to the relaxation phenomenon. In the intermediate temperature range, as the temperature decreases the intrachain correlation length (size of the domain) increases until at $T = T_N =$ 9·5 K three-dimensional long-range order sets in. At this point the correlations along the ZC's increase to infinity and a long-range order between the ZC's sets in. At temperatures slightly above T_N the ferromagnetic correlation within each chain, ferromagnetic domain, are of some finite length. Therefore, when the coupling between the chains sets in, it induces an emergence of a large contribution to the magnetic scattering at the Bragg angle as exhibited by the abrupt change in the magnetization curve (Fig. 3) at T_N.

References

AMIT, M., HOROWITZ, A. & MAKOVSKY, J. (1974). *Isr. J. Chem.* **12**, 827–830.

GUREWITZ, E., HOROWITZ, A. & SHAKED, H. (1979). *Phys. Rev. B*, **20**, 4544–4549.

GUREWITZ, E., MAKOVSKY, J. & ATZMONY, U. (1976). *Phys. Rev. B*, **13**, 375–378.

GUREWITZ, E., MAKOVSKY, J. & SHAKED, H. (1974). *Phys. Rev. B*, 9, 1071–1076.

GUREWITZ, E. & SHAKED, H. (1972). *Acta Cryst.* A**28**, 280–284.

WATSON, R. E. & FREEMAN, A. J. (1961). *Acta Cryst.* **14**, 27–37.

WYCKOFF, R. W. G. (1964). *Crystal Structures*, Vol. 2, 2nd ed., p. 430. New York: John Wiley.

Acta Cryst. (1982). B**38**, 2775–2781

The Preparation and Structure of Barium Uranium Oxide $BaUO_{3+x}$

BY S. A. BARRETT

*Inorganic Chemistry Laboratory, South Parks Road, Oxford OX*1 3*QR, England*

A. J. JACOBSON

Exxon Research and Engineering Co., PO Box 45 *Linden, New Jersey* 07036, *USA*

B. C. TOFIELD

*AERE, Harwell, Didcot, Oxfordshire OX*11 0*RA, England*

AND B. E. F. FENDER

Institut Laue–Langevin, 156*X Centre de Tri,* 38042 *Grenoble, France*

(*Received* 5 *February* 1982; *accepted* 10 *May* 1982)

Abstract

The structure of O-excess perovskite $BaUO_{3+x}$ has been examined by powder neutron diffraction at room temperature. The non-stoichiometry is clearly shown to arise from an equivalent number of Ba and U vacancies in a compound of overall composition $BaUO_{3\cdot30(3)}$. As expected, the temperature factors are larger in the disordered compound than in a compound close to the stoichiometric ideal of $BaUO_3$ which has also been structurally refined. A previous report that $BaUO_3$ is at least partially oxidized at room temperature in oxygen is confirmed. [$BaUO_{3\cdot30}$: *Pnma*, $a = 6\cdot2094$ (13), $b = 8\cdot7987$ (19), $c = 6\cdot2370$ (15) Å, $R_p = 16\cdot0\%$, $R_w = 13\cdot9\%$, $R_{exp} = 13\cdot1\%$ for 252 overlapping reflections; $Ba_{0\cdot98}UO_3$: *Pnma*, $a = 6\cdot1999$ (31), $b = 8\cdot7644$ (64), $c = 6\cdot2075$ (35) Å, $R_p = 8\cdot7\%$, $R_w = 10\cdot1\%$, $R_{exp} = 4\cdot2\%$ for 540 overlapping reflections.

Introduction

Ternary uranium oxide systems, are, in general, complex. Most of the known phases have been prepared by reactions of the stoichiometric metal oxides (or carbonates *etc.*) with one of the stoichiometric uranium oxides, but there is often a question whether the reported 'phases' are always discrete stoichiometric compounds or whether they are frequently (particularly at high temperature) simply

0567-7408/82/112775-07$01.00